Pramana – J. Phys. (2019) 92:76
https://doi.org/10.1007/s12043-019-1739-x

High-sensitivity measurement of Rydberg population via two-photon excitation in atomic vapour using optical heterodyne detection technique

ARUP BHOWMICK*, DUSHMANTA KARA and ASHOK K MOHAPATRA

School of Physical Sciences, National Institute of Science Education and Research Bhubaneswar, HBNI, P.O. Jatni, Khurda 752 050, India
*Corresponding author. E-mail: arup.b@niser.ac.in

MS received 16 January 2018; revised 28 September 2018; accepted 25 October 2018;
published online 13 March 2019

Abstract. We demonstrate a technique based on optical heterodyne detection to measure the Rydberg population in the thermal atomic vapour. The technique used a probe beam far off-resonant to the D2 line of rubidium along with a reference beam with frequency offset by 800 MHz in the presence of a coupling laser that couples to Rydberg state via two-photon resonance. The polarisation of the probe, reference and coupling beams are suitably chosen such that only the probe beam goes through a nonlinear phase shift due to the two-photon process which is measured relative to the phase shift of the reference beam using optical heterodyne detection technique. We show that the technique has a sensitivity to measure the minimum phase shift of the order of a few μrad. We have used a suitable model of two-photon excitation of a three-level atom to show that the minimum phase shift measured in our experiment corresponds to the Rydberg population of the order of 10^{-5}. The corresponding probe absorption for the given laser parameters is of the order of 10^{-7}. We demonstrate that this technique is insensitive to polarisation impurity or fluctuations in the beams. The technique is particularly useful in measuring the Rydberg population via two-photon excitation in thermal vapour where microchannel plates (MCP) could be relatively difficult to implement. It can also be used in the ultracold atomic sample with suitable laser parameters.

Keywords. Heterodyne; Rydberg population; two-photon; atomic vapour; dispersion.

PACS Nos **42.50.Nn; 32.80.Rm; 42.50.Gy; 34.20.Cf**

1. Introduction

Rydberg atoms are enriched with enhanced many-body interactions. When atoms in a densely frozen ensemble are excited to the Rydberg state using narrow-band lasers, strong Rydberg–Rydberg interactions lead to excitation blockade. This blockade interaction generates a highly entangled many-body quantum state in an ensemble of atoms which has become the basis for fundamental quantum gates using atoms [1–4] or photons [5] and for the realisation of single-photon sources [6,7]. Multiwave mixing process using electromagnetically-induced transparency (EIT) [8–10] and four-wave mixing dipole soliton in laser-induced atomic grating have been investigated theoretically and experimentally [11]. Ionisation of Rydberg atoms using half-cycle pulses has also been investigated theoretically [12]. Rydberg blockade in ultracold atoms and Bose–Einstein condensate (BEC) has been proposed [13–16] and observed [17] in magneto-optical trap [18–33]. It has significant application in simulating many-body phenomena [32] and generating entangled states [34] which are essential for quantum engineering [35]. Hence, it is important to develop a detection mechanism for Rydberg excitation. A direct absorption of the probe in two-photon resonance technique has been used for ultracold atoms to measure Rydberg population and the precision of the measurement is found to be 10^{-2} [36]. A state-selective spectroscopic detection of highly excited Rydberg population has also been reported [37]. Rydberg tomography of ultracold atoms has been established to image Rydberg blockade [38]. Study of Rydberg excitation in thermal atomic vapour has been reported in a number of literatures [39–44] in the context of the development of quantum engineering using the system. In the experiments with the cold atomic ensemble, microchannel plates (MCPs) are normally used to detect Rydberg atoms after ionisation using a DC electric field which

could be an issue with thermal vapour experiments due to the presence of charges sticking to the dielectric surface. Although a recent experiment with electrically contacted thermal vapour cell was used [45], all optical techniques are relatively easy to study the Rydberg excitation in the thermal vapour. Rydberg excitation using all-optical techniques are demonstrated in EIT regime in thermal vapour cell [39,46,47] and in micron-sized vapour cell [48]. Also, Rydberg excitation with two- and three-photon excitation has been studied in a large probe absorption regime [41,49]. In this paper, we present a method based on optical heterodyne detection technique to measure the dispersion of a probe beam due to two-photon excitation to Rydberg state in a small probe absorption regime. Heterodyne detection technique has been used to study the absorption and dispersion of coherent two-photon transition in an atomic ensemble [50], Zeeman coherence-induced anomalous dispersion [51] and enhanced Kerr nonlinearity in two-level atoms [46]. The technique has also been used to measure the cross phase modulation of a probe and a control beam in an N system using cold atoms [52–54] and also Rydberg EIT [47]. Here, we show with a suitable model that Rydberg population can be measured directly from the dispersion for a strong probe beam. We also show that the technique is insensitive to the small imperfections and fluctuations in the polarisation and intensity of the coupling laser. The technique is sensitive enough to measure probe absorption of the order of 10^{-7}.

2. Experimental methodology

The schematic diagram of the experimental set-up and the relevant energy level diagram are shown in figure 1. A technique based on optical heterodyne detection is used to measure the dispersion of a probe beam due to two-photon excitation to Rydberg state. The experimental set-up is similar to our earlier experiment of studying the optical nonlinearity of Rydberg-EIT in thermal vapour [47]. A probe beam along with a reference beam was derived from an external cavity diode laser operating at 780 nm. A frequency offset of 800 MHz was introduced between the probe and the reference beams by passing them through two acousto-optic modulators. Both beams were made to superpose using a polarising cube beam splitter (PBS). The interference beat signals were detected using two fast photodetectors by introducing polarisers at both the output ports of the PBS. A controlled relative phase can be introduced between both beat signals by using an optical phase shifter as explained in [47]. The probe beams coming out of one of the output ports of the PBS propagate through a magnetically shielded rubidium vapour cell. The temperature of the vapour cell can be varied from 30 to 130°C using a heater which was controlled by a proportional integral derivative (PID) controller. With this range of temperature, the density of ^{85}Rb can be varied in the range of 1.7×10^{10}–3.0×10^{13} cm^{-3}. The coupling beam was derived from a frequency doubled laser system operating at wavelength in the range of 478−482 nm and

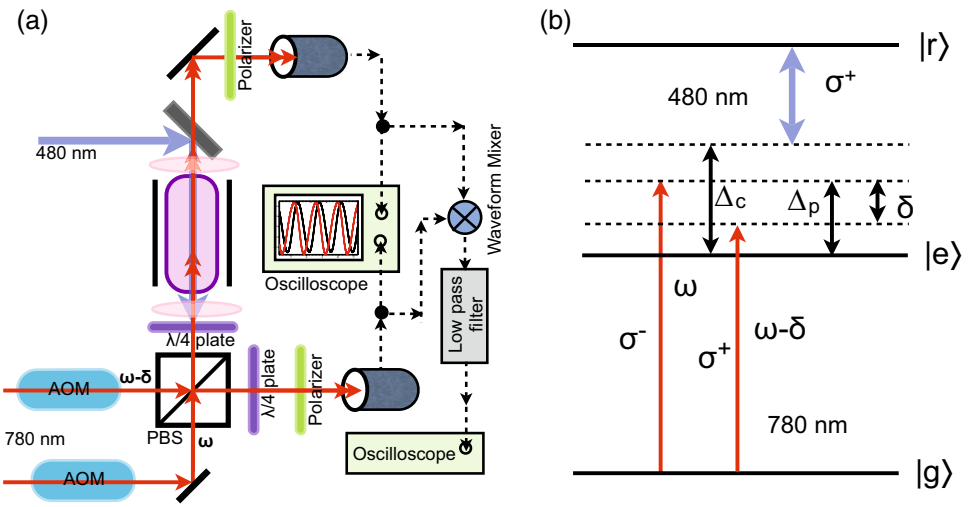

Figure 1. (**a**) Schematic diagram of the experimental set-up. (**b**) Energy level diagram for two-photon transition to the Rydberg state. Two probe beams with σ^+ and σ^- polarisations couple the transition $5S_{1/2}$, $F = 3(|g\rangle) \rightarrow 5P_{3/2}(|e\rangle)$ of ^{85}Rb. The coupling laser with σ^+ polarisation couples the transition $5P_{3/2}(|e\rangle) \rightarrow nS_{1/2}(|r\rangle)$. The probe (coupling) detuning is Δ_p (Δ_c) and frequency offset between the probe beams is δ.

it counterpropagates the probe beams through the cell. The coupling and the probe beams were focussed inside the cell using suitable lenses. The waist and the Rayleigh range of the probe (coupling) beams are 35 μm (50 μm) and 12 mm (10 mm), respectively. The peak Rabi frequencies of the laser beams and their variations over the length of the vapour cell were calculated [55] using the same parameters of the beams and were included in the theoretical model to fit all the experimental data.

The probe and the reference beams propagating through the medium can undergo different phase shifts by choosing suitable polarisations of the probe, reference and the coupling beams. The polarisation of the coupling beam was chosen to be σ^+. The reference beam with σ^+ polarisation cannot couple to the transition, $5S_{1/2} \rightarrow nS_{1/2}$ and does not go through any phase shift due to two-photon process. However, the probe beam with σ^- polarisation can couple the same two-photon transition and hence, goes through a phase shift due to two-photon excitation to the Rydberg state. This additional phase shift of the probe beam appears as a phase shift in the respective beat signal and is measured by comparing with the phase of the reference beat signal detected at the other output port of the PBS. As both beat signals are the outputs of the same interferometer, the noise due to vibration and acoustic disturbances is strongly suppressed. The signal-to-noise ratio was further improved by using a lock-in amplifier. A mechanical chopper was used to modulate the intensity of the coupling beam at a rate of 6 kHz which is used as the reference to the lock-in amplifier.

The output signal observed in the experiment is $S_L \propto \Re(\chi_{3L})$, where χ_{3L} is the susceptibility of the probe field due to the two-photon process [47]. In the experiment, the probe beam was stabilised at 1.3 GHz blue detuned to the D2 line of ^{85}Rb. With this detuning, the absorption of the probe beam is negligible due to the interaction with the D2 line at 130°C. The coupling laser frequency was scanned to observe the dispersion of the signal probe beam by measuring its phase shift due to the two-photon excitations to the Rydberg state. We have observed that the simple model of a three-level atom interacting with the probe and the coupling beams matches well with the measurement using this technique if the frequency offset is much larger than the reference Rabi frequency [47]. Hence, a large frequency offset of 800 MHz was used in the experiment.

3. Theory

The typical dispersion spectrum of the probe beam due to two-photon process is shown in figure 2. Two-photon resonance peaks corresponding to the transitions

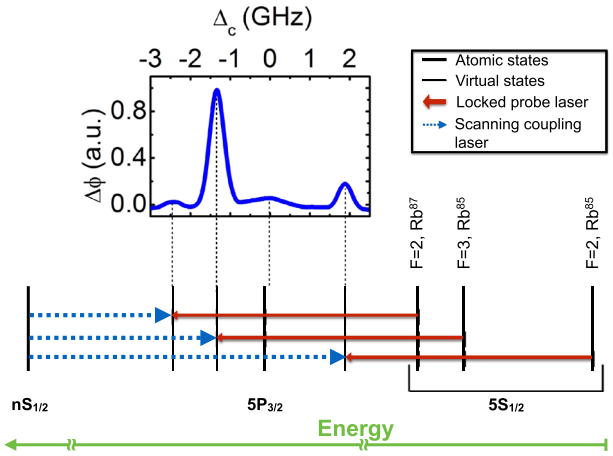

Figure 2. Typical dispersion spectrum observed in the experiment by scanning the coupling laser over 5 GHz. The induced nonlinear phase shift in the probe beam is measured due to two-photon coupling to the Rydberg state with principal quantum number $n = 33$. The peak Rabi frequencies of the coupling and the probe beam used for this spectrum are 24 and 400 MHz, respectively. The peaks corresponding to the transitions $5s_{1/2}(F = 2, 3) \rightarrow 5p_{3/2}$ of ^{85}Rb and $5s_{1/2}(F = 3) \rightarrow 5p_{3/2}$ of ^{87}Rb along with the respective energy levels are depicted.

$5s_{1/2}F = 3 \rightarrow ns_{1/2}$ and $5s_{1/2}F = 2 \rightarrow ns_{1/2}$ of ^{85}Rb and $5s_{1/2}F = 2 \rightarrow ns_{1/2}$ of ^{87}Rb are observed while the coupling beam is scanned over 5 GHz. The dispersion peak corresponding to the $5s_{1/2}F = 3 \rightarrow ns_{1/2}$ transition of ^{85}Rb was analysed for further study of Rydberg excitation. A usual dispersion profile of the two-photon resonance is observed for a weak probe beam as shown in figure 3a. However, an absorption-like dispersion profile is observed for a stronger probe beam as shown in figure 3b. In order to model the observed dispersion spectrum in the experiment, we consider a Hamiltonian of a three-level atom interacting with the probe and the coupling beams. Using rotating wave approximation in a suitable rotating frame, $H = -\frac{\hbar}{2}[(\Omega_p|e\rangle\langle g| + \Omega_c|r\rangle\langle e|) + \text{h.c.}] - \hbar[(\Delta_p - k_p v)|e\rangle\langle e| + (\Delta_2 + \Delta k v)|r\rangle\langle r|]$, where Ω_p (Ω_c) is the probe (coupling) Rabi frequency and Δ_p (Δ_c) is the probe (coupling) laser detuning with the two-photon detuning being $\Delta_2 = \Delta_p + \Delta_c$. k_p (k_c) is the wave vector of the probe (coupling) laser, $\Delta k = k_c - k_p$ and v is the velocity of the atom. The density matrix equation of the system, $i\hbar\dot{\hat{\rho}} = [\hat{H}, \hat{\rho}] + i\hbar\mathcal{L}_D\hat{\rho}$ are solved numerically in steady state. Here, $\mathcal{L}_D$ is the Lindblad operator which takes care of the decoherence in the system. In the numerical calculation, we have used the decay rates of the channels $|e\rangle \rightarrow |g\rangle$ and $|r\rangle \rightarrow |e\rangle$ as $2\pi \times 6$ and $2\pi \times 0.01$ MHz, respectively. A population decay rate of the Rydberg state to the ground state denoted as

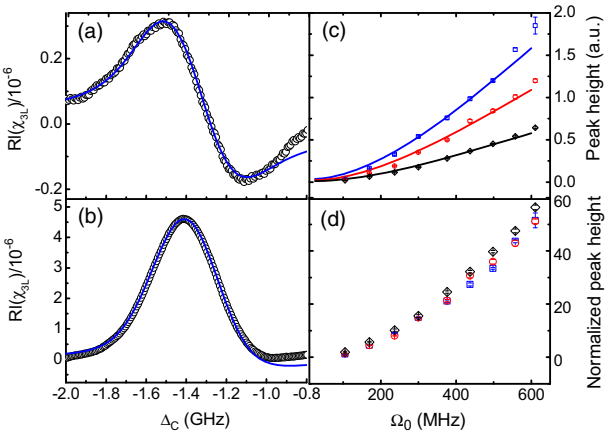

Figure 3. Refractive index of the signal probe beam propagating through the medium with coupling scanning over the two-photon resonance. The peak Rabi frequency of the coupling beam was 24 MHz and of the probe was (**a**) 60 MHz and (**b**) 400 MHz. The data points (○) represent the experimental measurement of dispersion and the solid lines are the corresponding curves generated from the theory. (**c**) Measured dispersion peak height as a function of peak Rabi frequency of the probe while coupling to the Rydberg state with $n = 33$ with atomic vapour densities 2.5×10^{12} cm^{-3} (◇), 1.25×10^{13} cm^{-3} (○) and 3.0×10^{13} cm^{-3} (□). The solid lines are the fitting using the theoretical model and a multiplication factor is used as the only fitting parameter which can be accounted for the overall gain in the experiment. (**d**) Dispersion peak height normalised to the peak height of a weak probe beam.

Γ_{rg} is used to account for the finite transit time of the thermal atoms in the laser beams. The dipole ρ_{rg} dephases at a rate of $(\Gamma_{rg}/2) + \gamma_{rel}$, where γ_{rel} accounts for the relative laser noise between the probe and the coupling beams. Γ_{rg} and γ_{rel} are of the order of $2\pi \times 0.5$ MHz. The susceptibility of the probe beam can be written as $\chi = \chi_{2L} + \chi_{3L}$, where χ_{2L} is due to the interaction of the probe with the $5s_{1/2} \rightarrow 5p_{3/2}$ transition in the absence of the coupling laser and χ_{3L} is due to the two-photon process in the presence of the coupling laser. χ_{2L} introduces only a DC offset in the phase of the probe and hence a DC offset in the signal of optical heterodyne detection technique (OHDT). After subtracting the DC offset, the dispersion spectrum is observed only due to χ_{3L} while scanning the coupling laser. The susceptibility of the probe beam due to two-photon process averaged over the thermal motion of the atoms can be calculated as

$$\chi_{3L} = \frac{2N|\mu_{eg}|^2}{\epsilon_0 \hbar \Omega_p} \frac{1}{\sqrt{\pi}\, v_p} \int_{-\infty}^{\infty} \rho_{eg}^{(3L)} e^{-(v^2/v_p^2)} dv, \qquad (1)$$

where v_p is the most probable speed of the atoms, N is the density and μ_{eg} is the dipole moment of the transition $|g\rangle \rightarrow |e\rangle$. $\rho_{eg}^{(3L)} = \rho_{eg} - \rho_{eg}^{(2L)}$, where $\rho_{eg}^{(2L)}$ is due to the interaction of the probe beam with the $|g\rangle \rightarrow |e\rangle$ transition in the absence of the coupling beam. The dispersion of the probe beam $\Re(\chi_{3L})$ calculated using the above theoretical model is compared with the experimental data as shown in figures 3a and 3b. The Doppler width of the two-photon resonance is roughly 250 MHz which is given by $\Delta k v_p$. As shown in figure 3b, the linewidth observed in the experiment is roughly 350 MHz. The higher linewidth observed in the experiment is attributed to the inhomogeneous light shift of the atoms with difference in velocities which contribute to the two-photon detuning.

In a further study, the variation of the dispersion peak height was measured as a function of probe Rabi frequency. The signal measured using the optical heterodyne detection technique is $S_L = 2A_s A_r \phi_s$ as discussed in [47]. Here ϕ_s is the nonlinear phase shift due to χ_{3L}. A_s and A_r are the signal and reference beat amplitudes contributing to the gain of the OHDT signal. During the experiment, the probe power is varied to study the intensity-dependent χ_{3L}. Variation in the probe intensity changes the beat amplitudes which ultimately leads to the variation in the gain of the OHDT signal. In order to keep the gain independent of the probe intensity, RF attenuators are used to adjust the beat amplitudes as constant throughout the experiment. The variation of the dispersion peak height as a function of probe Rabi frequency for different vapour densities is shown in figure 3c. The dispersion peak height calculated by the theoretical model for the same laser parameters and vapour density agrees well as shown in figure 3c. When the peak height data are normalised with the dispersion peak of a weak probe beam, then all the data corresponding to different densities fall on the same line as shown in figure 3d. This observation suggests that the refractive index of the medium depends linearly on the vapour density and the Rydberg–Rydberg interaction has negligible effect.

To get a further insight into the observed shape of the dispersion profile, we use the approximation $\Delta_p \gg \Gamma_{eg}, \Omega_p$ such that the intermediate state population is negligible. Then, in a regime $\Omega_p \gg \Gamma_{eg}$, we find

$$\Re(\rho_{eg}) = -\frac{\Omega_p}{2(\Delta_p - k_p v)} + \frac{1}{2(\Delta_p - k_p v)} [\Omega_p \rho_{rr} - \Omega_c \Re(\rho_{rg})]$$

from the density matrix equation. The first term in the above equation gives $\rho_{eg}^{(2L)} = -(\Omega_p/(2(\Delta_p - k_p v)))$ and the rest of the terms can be written as

$$\Re(\rho_{\mathrm{eg}}^{(3L)}) = \frac{1}{2(\Delta_{\mathrm{p}} - k_{\mathrm{p}}v)}[\Omega_{\mathrm{p}}\rho_{\mathrm{rr}} - \Omega_{\mathrm{c}}\Re(\rho_{\mathrm{rg}})]. \qquad (2)$$

ρ_{rr} and ρ_{rg} can be determined by approximating the three-level atom as an effective two-level atom by adiabatically eliminating the intermediate state [56] for the large single-photon detuning. In the regime, $\Omega_{\mathrm{p}} \gg \Omega_{\mathrm{c}}$, neglecting the second term in the above equation leads to $\Re(\rho_{\mathrm{eg}}^{(3L)}) \propto \rho_{\mathrm{rr}}$ and hence the dispersion gives rise to an absorption-like profile. For small Ω_{p}, contribution of the second term of the same equation gives a usual feature of dispersion profile as observed in the experiment. As dispersion is proportional to Rydberg population in a strong probe regime, this technique gives direct information about the Rydberg excitation and hence becomes an all-optical method to detect the Rydberg atoms. To measure the sensitivity of the technique, we recorded the dispersion signal with different coupling Rabi frequency as shown in figure 4. Using the effective two-level atom, Rydberg population can be determined as

$$\rho_{\mathrm{rr}} = \frac{\Omega_{\mathrm{eff}}^2}{\Delta_{\mathrm{eff}}^2 + 2\Omega_{\mathrm{eff}}^2 + \Gamma_{\mathrm{rg}}^2},$$

where

$$\Omega_{\mathrm{eff}} = \frac{\Omega_{\mathrm{p}}\Omega_{\mathrm{c}}}{2(\Delta_{\mathrm{p}} - \Delta_{\mathrm{c}})}$$

and

$$\Delta_{\mathrm{eff}} = 2(\Delta_{\mathrm{p}} + \Delta_{\mathrm{c}}) + 2\Delta k v + \frac{\Omega_{\mathrm{p}}^2}{(\Delta_{\mathrm{p}} - \Delta_{\mathrm{c}})}$$

which are the effective Rabi frequency and detuning of the approximated two-level atom, respectively. While the lasers are tuned within the Doppler width of the two-photon transition, the atoms with the velocity class resonant to the lasers contribute maximum to the Rydberg population. Using eqs (1) and (2), the peak of the dispersion due to two-photon process can be approximated as

$$\Re(\chi_{3L}) \approx \frac{\Omega_{\mathrm{eff}}}{2\sqrt{\pi}\Delta k v_{\mathrm{p}}} \frac{N|\mu_{\mathrm{eg}}|^2}{\epsilon_0 \hbar \Delta_{\mathrm{p}}} \rho_{\mathrm{rr}}.$$

Here, we have assumed that the peak of the dispersion corresponds to the atoms with zero velocity class within the effective Rabi frequency ($\Omega_{\mathrm{eff}}/\Delta k$) interacting resonantly with the lasers. From the above equation, the direct measurement of $\Re(\chi_{3L})$ from the phase acquired by the probe gives the measurement of the Rydberg population ρ_{rr}.

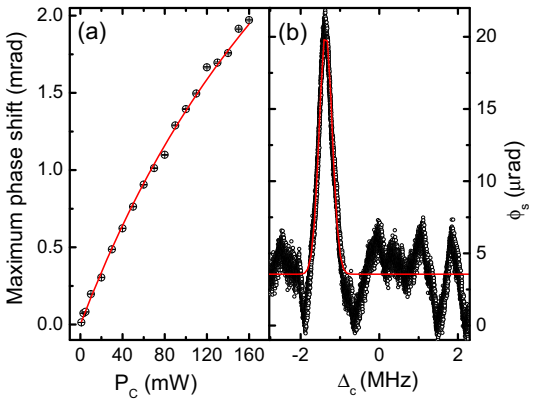

Figure 4. (**a**) Phase shift of the probe at the peak of the dispersion spectrum as a function of the coupling power. Open circles correspond to the measured phase shift using the heterodyne detection technique and the solid line is the fitting using the model discussed in the text. (**b**) Observed dispersion spectrum by scanning the coupling laser over the $5S_{1/2}(F = 3) \rightarrow nS_{1/2}$ transition of ^{85}Rb with coupling laser power being 1 mW. The signal is fitted with a Gaussian function to determine the phase shift at the peak of the spectrum.

4. Precision of the measurement

The phase shift (ϕ_{s}) due to the two-photon process measured using the heterodyne detection technique is related to the susceptibility as $\Re(\chi_{3L}) = 2\phi_{\mathrm{s}}/k_{\mathrm{p}}l$ where l is the length of the vapour cell. ϕ_{s} can be determined from the experimental set-up as $\phi_{\mathrm{s}} = V_{\mathrm{o}}/G\eta_{\mathrm{m}}$ where V_{o} and G are the output and overall gain of the lock-in amplifier used in the experiment, respectively. η_{m} is the sensitivity of the RF mixer which was determined by using two RF signals with a known phase difference with the same amplitudes as the beat signals of the heterodyne set-up in the experiment. The phase shift at the peak of the dispersion measured using the heterodyne detection technique by varying the coupling laser power is shown in figure 4a. The data were fitted with a simple formula which can be derived using the above analysis. The dispersion spectrum with very weak coupling power is shown in figure 4b and fitting with a Gaussian function gives the peak of the phase shift. Rydberg population can be determined from the measured phase shift as

$$\rho_{\mathrm{rr}} = \frac{2\epsilon_0 \hbar \Delta_{\mathrm{p}}}{N|\mu_{\mathrm{eg}}|^2} \frac{\Delta k v_{\mathrm{p}}}{\sqrt{\pi}\Omega_{\mathrm{eff}}} \frac{\lambda_{\mathrm{p}}}{l} \phi_{\mathrm{s}}.$$

The Rydberg population at the peak of the spectrum shown in figure 4b is found to be $\rho_{\mathrm{rr}} \approx 10^{-5}$.

In a further study of comparing this technique with the direct absorption measurement of the probe, the imaginary part of susceptibility can be calculated as

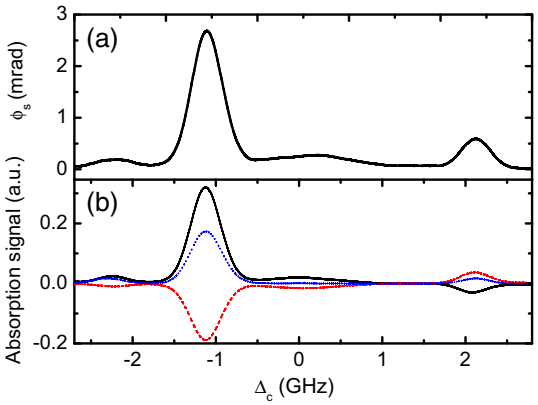

Figure 5. (**a**) Measured phase shift of the probe using heterodyne detection technique. (**b**) Observed signal from direct probe absorption measurement with coupling being σ^+ and probe being σ^-. The solid and the dashed curves correspond to the absorption of linear polarisation component in vertical and horizontal directions, respectively. The dotted curve corresponds to the total absorption of the probe light.

$$\Im(\chi_{3L}) = \frac{\Omega_{\text{eff}}}{\sqrt{\pi}\Delta k v_{\text{p}}} \frac{N|\mu_{\text{eg}}|^2}{\epsilon_0 \hbar} \left(\frac{\Gamma_{\text{rg}}}{\Omega_{\text{p}}^2}\right) \rho_{\text{rr}}.$$

The imaginary part is linked with the real part of susceptibility as $\Im(\chi_{3L}) = (2\Gamma_{\text{rg}}\Delta_{\text{p}}/\Omega_{\text{p}}^2)\Re(\chi_{3L})$. If $\Delta_{\text{p}} = 1$ GHz and $\Omega_{\text{p}} = 250$ MHz, then the phase shift $(k_{\text{p}} l \Re(\chi_{3L}))$ becomes two orders of magnitude larger compared to the absorption $(k_{\text{p}} l \Im(\chi_{3L}))$. In the experiment, direct absorption of the probe beam was measured with an improved sensitivity of the lock-in amplifier. The comparison of the direct probe absorption measurement with heterodyne detection technique is presented in figure 5. It has been observed that the direct probe absorption is very sensitive to the small change in the polarisation of the coupling and the probe beams. As shown in figure 5, the absorption of the orthogonal linear polarisation components of the σ^- light is opposite in sign and the total absorption is shown to be less compared to one of the linear polarisation component. Also, the signs of the absorption signals corresponding to different hyperfine states of the same spectrum are opposite to each other. The behaviour of the absorption spectrum observed from direct probe absorption measurement can only be explained by the small polarisation rotation of the probe field due to the impurity in the circular polarisation of the coupling laser beam. If $\rho_{\text{rr}} = 10^{-5}$, the probe absorption will be of the order of 10^{-7} for the given laser parameters and such a small absorption can easily be obscured in the polarisation rotation of the probe due to their small polarisation impurity due to non-ideal optical components. Hence, direct probe absorption measurement, in this case, cannot provide a reliable measurement of the Rydberg population for very small absorption. In contrast, the signal observed in heterodyne detection technique is insensitive to any small change in their polarisation. Hence, the observed dispersion signal giving the information about Rydberg population becomes robust and reliable.

5. Conclusion

In conclusion, we have demonstrated an all-optical technique to measure the two-photon excitation to Rydberg state. The technique is found to be sensitive enough to measure Rydberg population of the order of 10^{-7}. With such a small Rydberg population, direct absorption measurement cannot be reliable because it will be obscured by small polarisation rotation due to the imperfection in the polarisation components of light used in the experiment. The technique is particularly useful in the experiments with Rydberg excitation in the thermal vapour. However, the technique can also be used for ultracold atoms with suitable laser parameters.

Acknowledgements

The authors acknowledge Sushree S Sahoo and Snigdha S Pati for their assistance in performing the experiment. This experiment was financially supported by the Department of Atomic Energy, Government of India.

References

[1] D Jaksch, J I Cirac, P Zoller, S L Rolston, R Côté and M D Lukin, *Phys. Rev. Lett.* **85**, 2208 (2000)
[2] M D Lukin, M Fleischhauer, R Côté, L M Duan, D Jaksch, J I Cirac and P Zoller, *Phys. Rev. Lett.* **87**, 037901 (2001)
[3] L Isenhower, E Urban, X L Zhang, A T Gill, T Henage, T A Johnson, T G Walker and M Saffman, *Phys. Rev. Lett.* **104**, 010503 (2010)
[4] T Wilk, A. Gaëtan, C Evellin, J Wolters, Y Miroshnychenko, P Grangier and A Browaeys, *Phys. Rev. Lett.* **104**, 010502 (2010)
[5] I Friedler, D Petrosyan, M Fleischhauer and G Kurizki, *Phys. Rev. A* **72**, 043803 (2005)
[6] M Saffman and T G Walker, *Phys. Rev. A* **66**, 065403 (2002)
[7] Y O Dudin and A Kuzmich, *Science* **336**, 887 (2012)
[8] Y Du, Y Zhang, C Zuo, C Li, Z Nie, H Zheng, M Shi, R Wang, J Song, K Lu and M Xiao, *Phys. Rev. A* **79**, 063839 (2009)
[9] J Che, J Ma, H Zheng, Z Zhang, X Yao, Y Zhang and Y Zhang, *Europhys. Lett.* **109**, 33001 (2015)

[10] Z Zhang, J Che, D Zhang, Z Liu, X Wang and Y Zhang, *Opt. Express* **23**, 13814 (2015)

[11] Y Zhang, Z Wang, Z Nie, C Li, H Chen, K Lu and M Xiao, *Phys. Rev. Lett.* **106**, 093904 (2011)

[12] S Chatterjee, A Saha and B Talukdar, *Pramana – J. Phys.* **86**, 861 (2016)

[13] H Weimer, R Löw, T Pfau and H P Büchler, *Phys. Rev. Lett.* **101**, 250601 (2008)

[14] T Pohl, E Demler and M D Lukin, *Phys. Rev. Lett.* **104**, 043002 (2010)

[15] G Pupillo, A Micheli, M Boninsegni, I Lesanovsky and P Zoller, *Phys. Rev. Lett.* **104**, 223002 (2010)

[16] N Henkel, R Nath and T Pohl, *Phys. Rev. Lett.* **104**, 195302 (2010)

[17] A Angelone, F Mezzacapo and G Pupillo, *Phys. Rev. Lett.* **116**, 135303 (2016)

[18] D Tong, S M Farooqi, J Stanojevic, S Krishnan, Y P Zhang, R Côté, E E Eyler and P L Gould, *Phys. Rev. Lett.* **93**, 063001 (2004)

[19] K M Singer, M Reetz-Lamour, T Amthor, L G Marcassa and M Weidemüller, *Phys. Rev. Lett.* **93**, 163001 (2004)

[20] T Cubel Liebisch, A Reinhard, P R Berman and G Raithel, *Phys. Rev. Lett.* **95**, 253002 (2005)

[21] T Vogt, M Viteau, J Zhao, A Chotia, D Comparat and P Pillet, *Phys. Rev. Lett.* **97**, 083003 (2006)

[22] R Heidemann, U Raitzsch, V Bendkowsky, B Butscher, R Löw, L Santos and T Pfau, *Phys. Rev. Lett.* **99**, 163601 (2007)

[23] U Raitzsch, V Bendkowsky, R Heidemann, B Butscher, R Löw and T Pfau, *Phys. Rev. Lett.* **100**, 013002 (2008)

[24] E Urban, T A Jojnson, T Henage, L Isenhower, D D Yavuz, T G Walker and M Saffman, *Nature Phys.* **5**, 110 (2009)

[25] A Gaëtan, Y Miroshnychenko, T Wilk, A Chotia, M Viteau, D Comparat, P Pillet, A Browaeys and P Grangier, *Nature Phys.* **5**, 115 (2009)

[26] Y O Dudin, L Li, F Bariani and A Kuzmich, *Nature Phys.* **8**, 790 (2012)

[27] P Schauss, M Cheneau, M Endres, T Fukuhara, S Hild, A Omran, T Pohl, C Gross, S Kuhr and I Bloch, *Nature* **491**, 87 (2012)

[28] J D Pritchard, D Maxwell, A Gauguet, K J Weatherill, M P A Jones and C S Adams, *Phys. Rev. Lett.* **105**, 193603 (2010)

[29] T Peyronel, O Firstenberg, Q-Y Liang, S Hofferberth, A V Gorshkov, T Pohl, M D Lukin and V Vuletiċ, *Nature* **488**, 57 (2012)

[30] O Firstenberg, T Peyronel, Q-Y Liang, A V Gorshkov, M D Lukin and V Vuletié, *Nature* **502**, 71 (2013)

[31] V Parigi, E Bimbard, J Stanojevic, A J Hilliard, F Nogrette, R Tualle-Brouri, A Ourjoumtsev and P Grangier, *Phys. Rev. Lett.* **109**, 233602 (2012)

[32] T M Weber, M Höning, T Niederprüm, T Manthey, O Thomas, V Guarrera, M Fleischhauer, G Barontini and H Ott, *Nature Phys.* **11**, 157 (2015)

[33] Y-Y Jau, A M Hankin, T Keating, I H Deutsch and G W Biedermann, *Nature Phys.* **12**, 71 (2016)

[34] D Cano and J Fortágh, *Phys. Rev. A* **80**, 043413 (2014)

[35] H Labubu, S Ravels, D Barredo, L. Béguin, F Nogrette, T Lahaye and A Browaeys, *Phys. Rev. A* **90**, 023415 (2014)

[36] F Karlewski, M Mack, J Grimmel, N Sádor and J Fortágh, *Phys. Rev. A* **91**, 043422 (2015)

[37] W Sandner, G A Ruff, V Lange and V Eichmann, *Phys. Rev. A* **32**, 3794 (1985)

[38] M M Valado, N Malossi, S Scotto, D Ciampini, E Arimondo and O Morsch, *Phys. Rev. A* **88**, 045401 (2013)

[39] A K Mohapatra, T R Jackson and C S Adams, *Phys. Rev. Lett.* **98**, 113003 (2007)

[40] A K Mohapatra, M G Bason, B Butscher, K J Weatherill and C S Adams, *Nature Phys.* **4**, 890 (2008)

[41] C Carr, R Ritter, C G Wade, C S Adams and K J Weatherill, *Phys. Rev. Lett.* **111**, 113901 (2013)

[42] T Baluktsian, B Huber, R Löw and T Pfau, *Phys. Rev. Lett.* **110**, 123001 (2013)

[43] A K Kölle, G Epple, H. Kübler, R Löw and T Pfau, *Phys. Rev. A* **85**, 063821 (2012)

[44] Z Zhang, H Zheng, X Yao, Y Tian, J Che, X Wang, D Zhu, Y Zhang and M Xiao, *Sci. Rep.* **5**, 10462 (2015)

[45] D Barredo, H Kübler, R Daschner, R Löw and T Pfau, *Phys. Rev. Lett.* **110**, 123002 (2013)

[46] A M Akulshin, A I Sidorov, R J McLean and P Hannaford, *J. Opt. B: Quantum Semiclass Opt.* **6**, 491 (2004)

[47] A Bhowmick, S S Sahoo and A K Mohapatra, *Phys. Rev. A* **94**, 023839 (2016)

[48] H Kübler, J P Shaffer, T Baluktsian, R. Löw and T Pfau, *Nature Photon.* **4**, 112 (2010)

[49] O Firstenberg, C S Adams and S Hofferberth, *J. Phys. B: At. Mol. Opt. Phys.* **49**, 152003 (2016)

[50] G Müller, A Witch, R Rinkleff and K Danzmann, *Opt. Commun.* **127**, 37 (1996)

[51] A M Akulshin, S Barreiro and A Lezama, *Phys. Rev. Lett.* **83**, 4277 (1999)

[52] H Kang and Y Zhu, *Phys. Rev. Lett.* **91**, 093601 (2003)

[53] H Y Lo, P C Su and Y F Chen, *Phys. Rev. A* **81**, 053829 (2010)

[54] Y Han, J Xiao, Y Liu, C Zhang, H Wang, M Xiao and K Peng, *Phys. Rev. A* **77**, 023824 (2008)

[55] The probe Rabi frequency is estimated using the relation with the intensity of probe as $I/I_{\text{sat}} = 2|\Omega_{\text{p}}|^2/\Gamma^2$. For ^{85}Rb, $I_{\text{sat}} = 1.64\,\text{mW/cm}^2$ and $\Gamma = 2\pi \times 6\,\text{MHz}$. Coupling Rabi frequency is estimated by fitting the Rydberg EIT signal with a weak probe beam without focussing and then scaling it with the intensity of the beam

[56] R Han, H K Ng and B G Englert, *J. Mod. Opt.* **60**, 255 (2013)